



# Combustion characteristics of pelletized-biomass fuels: a thermogravimetric analysis and combustion study in a fluidized-bed combustor

Poramet Arromdee<sup>1</sup> · Pichet Ninduangdee<sup>2</sup>

<sup>1</sup> Laboratory of Advanced Combustion Technology and Energy Systems (LACTES), Department of Mechanical Engineering, Faculty of Engineering and Industrial Technology, Silpakorn University, Nakhon Pathom 73000, Thailand

<sup>2</sup> Division of Mechanical Engineering, Faculty of Engineering and Industrial Technology, Phetchaburi Rajabhat University, Phetchaburi 76000, Thailand

Received: 25 February 2022 / Revised: 20 September 2022 / Accepted: 16 November 2022 / Published online: 3 December 2022

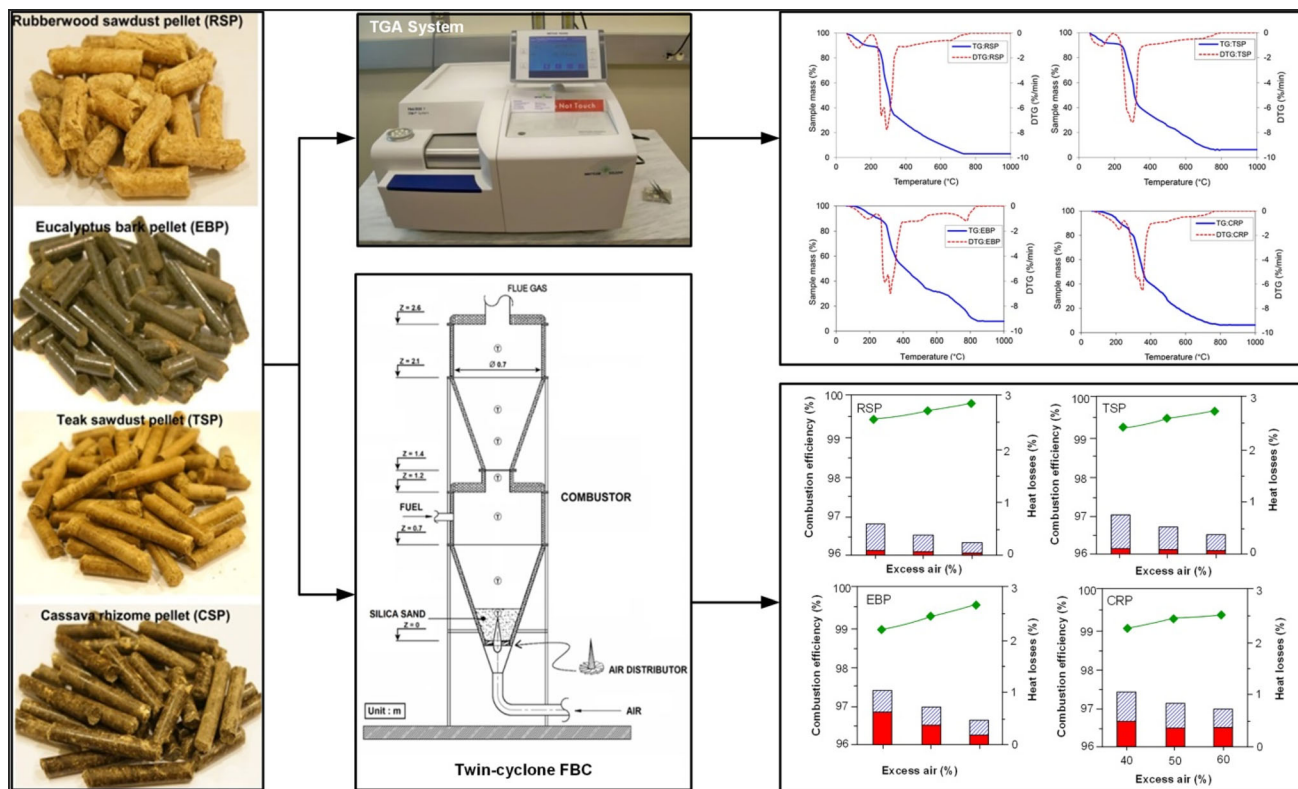
© The Joint Center on Global Change and Earth System Science of the University of Maryland and Beijing Normal University 2022

**Abstract** This work aimed to investigate the combustion characteristics of rubberwood sawdust pellet (RSP), teak sawdust pellet (TSP), eucalyptus bark pellet (EBP), cassava rhizomes pellet (CRP), and their corresponding raw biomass. The experiments were performed in a thermogravimetric (TG) analyzer and a fluidized-bed combustor (FBC). Thermogravimetric analysis (TGA) was conducted in the temperature range of 30–1000 °C at a heating rate of 10 °C/min in a dry air atmosphere. The combustion experiments were conducted in a twin-cyclone FBC at 120 kilowatts ( $kW_{th}$ ) heat input with three values of excess air (EA): 40, 50, and 60%. The combustion reactivity of the pellets was lower than raw biomasses, as indicated by higher values of peak, ignition, and burnout temperatures, as well as a lower comprehensive performance index value.

The activation energies of the biomass pellets were greater than the as-received biomasses, indicating that the biomass pellets required higher energy and temperature and a longer time for complete combustion. The pellet fuels had a higher residence time and better mixing of the fuel and bed particles, leading to higher combustion intensity in a fluidized bed. Carbon monoxide (CO), hydrocarbon ( $C_xH_y$ ), and nitric oxide (NO) emissions of the combustor when firing the pellets were lower compared to the burning of as-received biomasses. When firing the pellets at optimal EA (about 40%), the combustor operated at high combustion efficiency of 99.0–99.8%. This study indicated that the biomass pellets have desirable combustion characteristics that could be used as alternative fuels for sustainable energy production.

✉ Pichet Ninduangdee  
ninduangdee.p@gmail.com; pichet.nin@mail.pbru.ac.th

## Graphical Abstract



**Keywords** Biomass · Thermogravimetric analysis · Fluidized-bed combustion · Combustion efficiency · Emissions

## List of symbols

A	Ash content in fuel (wt.%)
A	Pre-exponential factor
C	Carbon content in fuel (wt.%)
$C_{fa}$	Unburned carbon content in fly ash (wt.%)
CO	Carbon monoxide (ppm)
CR	Cassava rhizomes
CRP	Cassava rhizomes pellet
$C_xH_y$	Hydrocarbon (ppm)
DTG	Differential thermogravimetric
$DTG_{max}$	Maximum burning rate (%/min)
$DTG_{mean}$	Average weight loss rate (%/min)
$E_a$	Activation energy (kJ/mol)
EA	Excess air (%)
EB	Eucalyptus bark
EBP	Eucalyptus bark pellet
FBC	Fluidized-bed combustor
FC	Fixed carbon content in fuel (wt.%)
H	Hydrogen content in fuel (wt.%)
LHV	Lower heating value, kJ/kg
$m_\tau$	Actual mass (at time $\tau$ ) of the sample (kg)

$m_0$	Initial mass of the sample (kg)
$m_f$	Final mass of the sample (kg)
$n$	Reaction order
N	Nitrogen content in fuel (wt.%)
NO	Nitric oxide, ppm
O	Oxygen content in fuel (wt.%)
$q_{ic}$	Heat loss due to incomplete combustion (%)
$q_{uc}$	Heat loss due to unburned carbon (%)
$r$	Correlation coefficient
RS	Rubberwood sawdust
RSP	Rubberwood sawdust pellet
S	Sulfur content in fuel (wt.%)
$S_i$	Comprehensive performance index ( $\%^2/\text{min}^2 \cdot \text{°C}^3$ )
$T$	Absolute temperature (°C)
$T_b$	Burnout temperature (°C)
TG	Thermogravimetric
TGA	Thermogravimetric analysis
$T_{ig}$	Ignition temperature (°C)
$T_p$	Peak temperature (°C)
TS	Teak sawdust
TSP	Teak sawdust pellet
$u$	Superficial air velocity at the air distributor exit (m/s)
$u_{mff}$	Minimum velocity of full fluidization (m/s)
$V_{dg@6\% O_2}$	Volume of flue gas per 1 kg fuel on a dry basis and at 6% $O_2$ ( $\text{m}^3/\text{kg}$ )

VM	Volatile matter in fuel, wt.%, on as received basis
W	Moisture content in fuel, wt.%, on as received basis
Z	Level along the combustor height above the air distributor, m

### Greek symbols

$\alpha$	Mass conversion ratio
$\beta$	Heating rate ( $^{\circ}\text{C}/\text{min}$ )
$\eta_c$	Combustion efficiency (%)

## 1 Introduction

The recent energy and environmental crises have driven the energy sector to develop technologies using renewable and sustainable resources instead of using less environmentally friendly fossil fuels. Biomass is a green and clean renewable energy source. It can be considered as one of the few viable replacement options for fossil fuels due to its high availability, carbon dioxide neutrality, and low sulfur content (Rokni et al. 2018). Using biomass as fuel allows rapid technological adaptation of existing coal installations. Among the main thermochemical processes of energy conversion, combustion is the primary method for biomass energy conversion and accounts for over 90% of the world's bio-energy production (Malico et al. 2019).

Thailand has a strong agro-industry base that generates substantial wastes and residues from local agricultural and forest industries, which can be utilized as renewable energy sources (biomass fuel) for producing heat and electricity. This country's total energy generation capacity from solid biomasses accounted for 1480 petajoules (PJ), as reported in 2020 (DEDE 2020). Some biomasses include rice husks, oil palm residues, wood chip and pellets, sugarcane residues (Martsri et al. 2021), and rubberwood (Wongsapai et al. 2020), already been utilized for heat production and power generation in Thailand. Other biomasses, including rubberwood sawdust (RS), teak sawdust (TS), eucalyptus bark (EB), and cassava rhizomes (CR), are also vital bioenergy resources and show potential for use as fuel in direct combustion systems. These biomasses have not been used as fuel yet because of their inherent physicochemical properties, such as non-uniform physical properties, excessive moisture content, low calorific value, and energy density. Therefore, these feedstocks need pretreatment to improve their quality for efficient conversion and utilization. If fully utilized, energy about 155 PJ can be recovered in Thailand (DEDE 2020).

One of the promising ways to improve the quality of the low-quality feedstocks is pelletization. This process transforms the raw or as-received biomasses into homogeneous

solid biofuel with higher bulk and energy densities, consequently leading to better handling, transportation, storage, and combustion efficiency. Tumuluru (2018) reported that the biomass pellets have low moisture content (below 10%), a calorific value of about 15–20 MJ/kg, and bulk density up to 750 kg/m<sup>3</sup>. The biomass pellets are generally made under mechanical pressure in an atmospheric environment. Mian et al. (2020) showed that the biomass's chemical structure and composition underwent insignificant changes after pelletization, but the physical structure, such as the biomass's porosity and surface morphology, changed substantially. As a result, the biomass pellet's thermal characteristic is expected to differ from the as-received feedstock.

Thermogravimetric analysis (TGA) is a helpful tool widely used for investigating thermal degradation behaviors and combustion characteristics of biomass feedstocks (Kongto et al. 2022; Saikia et al. 2018). Numerous research studies performed TGA to assess thermal degradation behaviors and combustion characteristics of different solid fuels, such as wood biomass, oat, sewage sludge (Magdziarz and Wilk 2013), waste capsicums, sawdust (Wang et al. 2012), cotton, forest residues, wood char, lignite, hard coal char (Kastanaki and Vamvuka 2006), palm shell, palm fiber, empty fruit bunches, sub-bituminous coal and their blends (Idris et al., 2012), peanut shells and tamarind shells (Kuprianov and Arromdee 2013), corn straw, corn straw pellet, pine and pine pellet (Mian et al. 2020), sludge pellet, camphor pellet, and sludge–camphor pellet (Jiang et al. 2015). Ninduangdee et al. (2015) found that biomass combustion in the TGA system was divided into three stages: (i) water evaporation, (ii) volatile release and its combustion, and (iii) char combustion. TGA also provides essential information for determining combustion kinetic parameters, which are helpful for efficient design of the reactors, optimization, and control of thermochemical processes. A short review of the literature regarding combustion characteristics and kinetics of various solid fuels using TGA is summarized in Table 1. The current work is the first report on the investigation of thermal degradation and combustion kinetics of RS, TS, EB, CR, and their corresponding pellets.

Fluidized-bed combustor (FBC) is suitable technique for burning biomasses such as agricultural residues, municipal solid waste, and sewage sludge. The combustion intensity in FBC is more significant than in a conventional combustion system, for example, a fixed-bed grate-firing system (Ninduangdee and Kuprianov 2018). With intensive and uniform particles mixing between bed material and biomass fuel, FBC ensures low carbon monoxide (CO) and nitric oxide (NO) emissions, and high combustion efficiency for burning various biomass fuels. The combustion efficiency of FBC fired with biomasses can be high, up to

**Table 1** Combustion study of different biomasses using TGA: literature review

Biomass	Experimental conditions	Kinetic model	Main findings	References
Wood biomass, oat, sewage sludge, and coal	Ambient temperature to 1000 °C, 15 mg sample, 10, 40, and 100 °C/min heating rate, and 100 mL/min air flow	Kissinger–Akahira–Sunose	The activation energies for coal, wood biomass, oat, and sewage sludge were 21–146, 81–223, 12–283, and 30–161 kJ/mol, respectively	Magdziarz and Wilk (2013)
Waste capsicums, sawdust, and coal	25–1400 °C, 6 mg sample, 10, 20, 30 °C/min heating rate, and 100 mL/min air flow	Coats-Redfern	The ignition characteristics of the biomass were better than that of coal. Activation energy for volatile combustion was 79 kJ/mol and 45 kJ/mol for char combustion	Wang et al. (2012)
Cotton, forest residues, and wood char	25–850 °C, 3–7 mg, 10 °C/min heating rate, and 100 mL/min air flow	Power law model	Biomass chars were generally more reactive than those of hard coal and lignite. Activation energies for forest residue, cotton residue, and wood char were 130, 150, and 145 kJ/mol, respectively	Kastanaki and Vamvuka (2006)
Palm shell, palm fiber, empty fruit bunches, and sub-bituminous coal, and their blends	25–1100 °C, 20 mg, 10, 20, 40 and 60 °C/min heating rate, 50 mL/min air flow	Iso-conversional method	Adding biomass to coal improved combustion reactivity of the fuel blend. Activation energy of coal, palm shell, fiber and empty fruit bunch and EFB combustion were $65 \pm 27$ , $139 \pm 49$ , $118 \pm 49$ , and $105 \pm 56$ kJ/mol, respectively	Idris et al. (2012)
Peanut and tamarind shells	Ambient temperature to 900 °C, 7–10 mg sample, 20 °C/min heating rate, and 60 mL/min air flow	Coats-Redfern	Tamarind shell with lower ignition temperature was ignited much easier than peanut shell. Activation energy of tamarind shell (33–84 kJ/mol) was lower than peanut shell (28–140 kJ/mol)	Kuprianov and Arromdee (2013)
Corn straw, corn straw pellet, pine and pine pellet	Room temperature to 1000 °C, 7–8 mg, 5, 10, and 15 °C/min heating rate, 100 mL/min air flow	Distributed Activation Energy	The activation energy of the raw biomass and pellet combustion were 98–229 and 119–244 kJ/mol, respectively. The activation energy for volatiles combustion was higher than char combustion	Mian et al. (2020)
Sludge pellet, camphor pellet, and sludge-camphor pellet	Ambient temperature to 800 °C, 5, 10, 20, and 40 °C/min heating rate, 100 mL/min air flow	Flynn–Wall–Ozawa and Starink	The average activation energy of sludge pellet, camphor pellet, and sludge-camphor pellet were 188, 129, and 159 kJ/mol, respectively	Jiang et al. (2015)

99%. Shimizu et al. (2006) showed that cotton stalk was fired effectively in a bubbling FBC with 99.5–99.8% combustion efficiency. As Quan et al. (2022) reported, FBC operated with 98–99% combustion efficiency when firing sewage sludge in the range of 800–850 °C. Duan et al. (2014) conducted a combustion experiment on burning pelletized peanut shells in a vortexing FBC. They found that the combustor operated at 98.0–98.6% combustion efficiency with low emissions of CO (less than 70 ppm) and NO (up to 114 ppm). Werther et al. (2000) found that CO emission from the FBC can be controlled by increasing excess, while NO emission can be reduced by lowering the amount of excess air. Experiments on firing various biomasses by Permchart and Koupryanov (2004) revealed similar effects of excess air on emissions of CO and NO. Ninduangdee and Kuprianov (2014) reported that the combustion and emission performances of the FBC

depended on fuel properties, operating conditions, and bed material type. Chirone et al. (2008) combusted biomass pellets in a bench-scale batch FBC. They observed that the pellets had a longer fuel devolatilization time than the original loose fuel constituents. This positive effect enhanced the combustion characteristics of FBC firing pellet fuels. Ninduangdee and Kuprianov (2018) investigated the combustion of rice husk pellet in a conical FBC. They observed that the rice husk pellet with heavy particles mainly combusted in a fluidized bed region, leading to high burnout and combustion efficiency.

The knowledge regarding thermal degradation and combustion characteristics, as well as combustion kinetic parameters of rubberwood sawdust pellet (RSP), teak sawdust pellet (TSP), eucalyptus bark pellet (EBP), and cassava rhizome pellet (CRP), has been still very limited. This information is crucial prior to using biomass pellets

for thermochemical processes. There is also limited information regarding the combustion characteristics of these biomass pellets in a practical combustion system, particularly in FBC.

The purpose of this work was to investigate the combustion characteristics of RSP, TSP, EBP, and CRP in a thermogravimetric (TG) analyzer and a pilot-scale FBC. The TGA was performed to assess the pelletized biomass's thermal decomposition under combustion condition. The characteristic temperatures of combustion, such as ignition ( $T_{ig}$ ), peak ( $T_p$ ), and burnout ( $T_b$ ), comprehensive performance index values ( $S_i$ ), and kinetic parameters were determined with the objective of assessing the thermal and combustion reactivity of the proposed biomasses. The combustion experiment was also conducted in FBC for a specified range of excess air (EA). Special attention was given to combustion behaviors inside the combustor and the effects of fuel properties and EA on major gaseous emissions and the combustor's combustion efficiency. The novelty of the present work is knowledge of (i) the thermal degradation behaviors, characteristic temperatures of combustion, and kinetic parameters of RSP, TSP, EBP, and CRP and (ii) combustion characteristics and performance of the twin-cyclone FBC when firing the proposed biomass pellets in the specified operating conditions.

## 2 Materials and methods

The working hypothesis for this study was that the pelletized biomasses (RSP, TSP, EBP, and CRP) could be efficiently utilized as a fuel in a combustion system. Two experimental series: (i) TGA and (ii) combustion tests in the twin-cyclone FBC were performed in order to test the hypothesis. In the first stage, the thermal decomposition, combustion characteristics, and kinetics of the proposed fuels were investigated by employing TGA. In the second series, RSP, TSP, EBP, and CRP were burned in a twin-cyclone FBC (Ninduangdee et al. 2020) for a specified range of the operating condition (i.e., EA) to investigate the combustion characteristics and performance of the combustor. The TGA and combustion experiments were also performed for the corresponding as-received biomasses to facilitate an interpretation of the main results. Materials and experimental facilities, and methods are explained in the following section.

### 2.1 Properties of feedstock

The selected biomass pellets: RSP, TSP, EBP, and CRP, used in this study were made by using a flat-die pellet pelletizer at room temperature. As-received biomasses: RS, TS, EB, and CR; were shredded in a shredder to reduce

particle size and then pulverized by a grinding machine, ensuring a particle size of up to 3 mm. During pellet making, no binders, chemicals, or additives were used. Each ground biomass, with a specified amount of water (10–15% by weight), was put into a 75 kW pelletizer which pressed the ground biomass into densified cylindrical pellets of 6 mm in diameter and up to 60 mm in length. After cooling by ambient air, the pellets were kept in fabric sacks and stored at room temperature to ensure stable fuel quality. The solid density of the pelletized biomasses was 1450–1650 kg/m<sup>3</sup>.

Table 2 shows the combustion-related properties, as well as the chemical structure of the raw feedstock and biomass pellets used in this study. The proximate analysis was determined following ASTM standards: ASTM E871 for fuel moisture (W), ASTM E872 for volatile matter (VM), and ASTM E1755 for ash content (A), whereas fixed carbon (FC) was calculated by difference. The ultimate analysis of biomass components: carbon (C), hydrogen (H), nitrogen (N), and sulfur (S); were determined based on ASTM E777 (for C and H), ASTM E778 (for N), and ASTM E775 (for S), while oxygen content (O) was calculated by difference. The chemical structure of the fuels was obtained according to the method presented by Van Soest et al. (1991). From the data in Table 2, all the pelletized biomasses had improved fuel properties, e.g., lowered W content and VM, while increased FC, compared to the corresponding raw biomasses. The ultimate analysis indicated that C content in the pellets increased, whereas the O and H content decreased due to a reduction of moisture during the pelletization of the biomass. As a result, the lower heating value (LHV) of all biomass pellets was relatively higher than that of the raw feedstock. From Table 2, the S content in all biomasses was insignificant. The chemical constituents of both raw and pelletized biomasses were quite similar. This fact indicated a minor impact of pelletization on the fuel's chemical structure. The LHV of RSP, TSP, and CRP were relatively high at about 17–18 MJ/kg, while the LHV of EBP was about 15 MJ/kg. Note that the calorific values of tested biomasses were measured using an oxygen bomb calorimeter (1341 Plain Jacket Bomb Calorimeter equipped with a Parr 6775 digital thermometer, Parr Instrument Company, USA) following the ASTM D2015 standard test method. The LHV was determined from the higher heating value by subtracting latent heat of evaporation of water formed from fuel moisture and hydrogen content. All test data was repeated three times to ensure accuracy and reproducibility.



**Table 2** Properties of raw and pelletized biomasses used in the current work (W = fuel moisture; VM = volatile matter; FC = fixed carbon; A = fuel ash)

Sample	Ultimate analysis (as-received basis, wt.%)					Proximate analysis (as-received basis, wt.%)				Chemical structure (dry and ash-free basis, wt.%)			LHV (kJ/kg)
	C	H	O	N	S	W	VM	FC	A	Hemicellulose	Cellulose	Lignin	
<i>Raw biomass</i>													
RS	39.53	8.32	41.31	0.22	0.02	9.2	68.3	21.1	1.4	22.2	63.4	14.4	16,200
TS	37.32	9.94	40.12	0.22	–	9.1	69.1	18.5	3.3	1.8	69.3	28.9	16,600
EB	27.17	6.60	41.25	0.45	0.03	15.1	49.7	25.8	9.4	45.3	48.4	6.3	13,260
CR	38.38	7.68	39.19	1.12	0.03	9.5	69.5	16.9	4.1	19.2	54.9	25.9	15,560
<i>Biomass pellet</i>													
RSP	44.70	5.36	39.33	0.25	0.06	8.5	59.9	29.8	1.8	21.9	63.1	15.0	17,500
TSP	42.94	7.94	36.72	0.30	–	8.1	66.9	21.0	4.0	1.0	69.1	29.9	18,180
EBP	41.70	4.60	36.10	0.54	0.06	6.3	43.1	39.9	10.7	44.7	47.4	7.8	14,700
CRP	43.20	5.68	36.73	1.32	0.07	6.6	67.4	19.6	6.4	18.9	54.5	26.6	17,050

## 2.2 Thermogravimetric analysis

The TGA was performed in a thermogravimetric analyzer (TGA/DSC1-Mettler Toledo, Switzerland). The measurement precision for temperature was  $\pm 0.5$  °C, while the sensitivity of the microbalance was less than 1.0  $\mu\text{g}$ . Before the tests, an individual sample was carefully prepared from a cylindrical pellet to create a tablet-like shape (5 mm in diameter, 4 mm in height, and about 120 mg in mass). In each test, the individual sample was put in a 900  $\mu\text{L}$  aluminum crucible (pan) and heated from 30 to 1000 °C at a constant heating rate of 10 °C/min in a combustion environment. Dry air at a flow rate of 30 mL/min was used as a furnace medium. The thermal degradation behavior of the biomass sample was represented by the TG and differential thermogravimetric (DTG) curves. The TG curve shows the sample mass loss versus furnace temperature, whereas the DTG curve represents the time derivative of the sample mass loss.

Note that the TGA for the original biomasses was also conducted with the same heating and airflow rates as the main experiments. The as-received biomasses were ground to ensure fine particle sizes of about 200  $\mu\text{m}$ , with approximately 20 mg of sample used in each test. The obtained results were used to assist in an interpretation of the main results of this study. Triplicate tests were conducted for each fuel option to ensure the reproducibility of the findings.

The comprehensive performance index ( $S_i$ ) value was determined and then compared between the fuel options to evaluate the combustion performance of selected fuels. The index  $S_i$  is an integrated solid fuel ignition, combustion, and burnout characteristics. The greater value of  $S_i$  indicates better combustion characteristics and faster burnout

of the feedstock. The index  $S_i$  can be calculated as follows (Niu et al. 2016; Kongto et al. 2022):

$$S_i = \text{DTG}_{\max} \cdot \text{DTG}_{\text{mean}} / (T_{\text{ig}}^2 \cdot T_{\text{b}}) \quad (1)$$

where  $\text{DTG}_{\max}$  is the maximum burning rate (%/min);  $\text{DTG}_{\text{mean}}$  is the average weight loss rate (%/min);  $T_{\text{ig}}$  and  $T_{\text{b}}$  are the ignition and burnout temperatures (°C). The corresponding parameters in Eq. (1) were determined from the TG/DTG curves. Note that  $T_{\text{ig}}$  and  $T_{\text{b}}$  were determined according to the method recommended by Kuprianov and Arromdee (2013).

## 2.3 Kinetic models

The combustion kinetic parameters of the raw biomass feedstock and their pellets during combustion were analyzed using the methodology recommended by Coats and Redfern (1964). Following this method, the parameters of thermal events such as activation energy ( $E_a$ ), pre-exponential factor ( $A$ ), and reaction order ( $n$ ) can be calculated.

From the TG curve, the mass conversion ratio ( $\alpha$ ) can be defined as follows:

$$\alpha = \frac{m_0 - m_{\tau}}{m_0 - m_{\text{f}}} \quad (2)$$

where  $m_0$  is the initial mass of the sample,  $m_{\tau}$  is the actual mass (at time  $\tau$ ) of the sample, and  $m_{\text{f}}$  is the final mass of the sample.

The kinetic equation describing the biomass decomposition with respect to time can be written as:

$$\frac{d\alpha}{d\tau} = A \exp\left(-\frac{E_a}{RT}\right) (1 - \alpha)^n \quad (3)$$

where  $R$  is the universal gas constant ( $R = 8.314 \text{ J/mol}\cdot\text{K}$ ) and  $T$  is absolute temperature (K).

For a constant heating rate ( $\beta = \frac{dT}{dt} = \text{const.}$ ) TG experiments, Eq. (3) can be rewritten as:

$$\frac{d\alpha}{(1-\alpha)^n} = \frac{A}{\beta} \exp\left(-\frac{E_a}{RT}\right) dT \quad (4)$$

For the Coats and Redfern method, it is assumed that the value of  $2RT/E_a$  is much less than 1.0 in the combustion reactions and the value of  $E_a$  is constant. Thus, integration of Eq. (4) results:

$$\text{for } n = 1: \quad -\ln\left[-\frac{\ln(1-\alpha)}{T^2}\right] = -\ln\left[\frac{AR}{\beta E_a}\right] + \frac{E_a}{RT} \quad (5)$$

$$\text{for } n \neq 1: \quad -\ln\left[\frac{1-(1-\alpha)^{1-n}}{T^2(1-n)}\right] = -\ln\left[\frac{AR}{\beta E_a}\right] + \frac{E_a}{RT} \quad (6)$$

From Eqs. (5) and (6), one can observe the linear correlation if the left-hand side of Eqs. (5) and (6) are plotted versus  $1/T$ . The best fit with the highest correlation coefficient can be achieved when the  $n$  value is appropriately selected. Then, the kinetic constants:  $E_a$  and  $A$  can be calculated from the slope of the fitted line and the intercept term (i.e.,  $\ln(AR/\beta E_a)$ ), respectively.

## 2.4 Combustion study on firing raw and pelletized biomasses in FBC

A combustion study on burning the pelletized biomasses and their as-received biomasses was performed in a twin-cyclone FBC, as depicted in Fig. 1. The combustor's design and geometrical details have been described in the previous studies (Ninduangdee et al. 2020). This combustor had a compact design, allowing high-intensive burning of various kinds of solid fuel with different particle sizes and fuel properties. It comprised two cyclonic combustion chambers, with an identical configuration and geometrical characteristics, arranged co-axially and connected in series by a pipe with a 0.2 m inner diameter. The lower combustion chamber used a swirl motion from the annular spiral air distributor to ensure high-intensive burning of the biomass fuel, whereas the upper chamber was used to ensure complete combustion of the fuel burned and mitigate the major gaseous pollutants. A diesel oil-firing burner was used to preheat the bed material during the combustor start-up mode. Once the bed temperature reached approximately  $500 \text{ }^\circ\text{C}$ , which was higher than the ignition temperature of the selected fuels obtained from TGA, the burner was turned off. Then, the biomass was supplied into the lower combustor at a specified fuel feed rate using a screw-type fuel feeder at 0.9 m above the air distributor.

All test series were performed at a similar heat input of approximately  $120 \text{ kW}_{\text{th}}$  to the combustor with three specified amounts of excess air (EA): 40%, 50%, and 60%. An actual value of excess air was estimated according to Basu et al. (2000). During the trial under specified operating conditions, concentrations of  $\text{O}_2$  and major gaseous pollutants ( $\text{CO}$ ,  $\text{C}_x\text{H}_y$ , and  $\text{NO}$ ) were measured using a portable flue gas analyzer (Testo-350, Testo, Germany) at the stack. The measurement accuracies of the gas concentrations were:  $\pm 0.2 \text{ vol.}\%$  for  $\text{O}_2$ ,  $\pm 5\%$  for  $\text{CO}$  within the range of 200–2000 ppm,  $\pm 10\%$  for  $\text{CO}$  higher than 2000 ppm,  $\pm 10\%$  for  $\text{C}_x\text{H}_y$  (as  $\text{CH}_4$ ), and  $\pm 5\%$  for  $\text{NO}$ . The temperature and  $\text{O}_2$  concentration were measured along the radial direction in the combustor for the test at 50% excess air at five levels ( $Z$ ) above the air distributor: 0.45 m, 0.95 m, 1.30 m, 1.85 m, and 2.35 m. The combustion efficiency of the combustor was assessed for each test using the heat-loss method provided in Appendix A.

Quartz sand, with a particle size of 0.3–0.5 mm and a solid density of  $2500 \text{ kg/m}^3$ , was used as the bed material in the reactor. During all combustion tests, the bed material was maintained at a 20 cm height (under static conditions). For the selected bed material and bed height, the value of the minimum velocity of full fluidization ( $u_{\text{mff}}$ ) was quantified as 0.8 m/s, ensuring a fully bubbling fluidized-bed regime with partial swirl motion (Ninduangdee et al. 2020). According to the methods recommended by Ninduangdee and Kuprianov (2018), the range of the superficial air velocity at the air distributor exit ( $u$ ) in the combustor when firing different fuel options at the lowest amount of excess air (i.e., EA = 40%) was predicted to be 1.2–1.6 m/s, which was higher than the above-mentioned  $u_{\text{mff}}$  value. Therefore, sustainable bed fluidization can be achieved during combustion of the selected biomasses for the range of excess air levels.

## 3 Results and discussion

### 3.1 Thermal decomposition of raw and pelletized biomasses

Figure 2 shows TG and DTG curves of the raw biomasses: RS, TS, EB, and CR; under an air atmosphere and heating rate of  $10 \text{ }^\circ\text{C}/\text{min}$ . When increasing the furnace temperature, the mass loss of the samples was due to the consecutive thermal decomposition of the biomass structural components, exhibiting some specific features at distinct temperatures determined using the boundary temperatures corresponding to the two neighbor minimums on the DTG curve. Haykiri-Acma et al. (2010) reported that the decomposition of hemicellulose occurs at relatively low temperatures (160–360  $^\circ\text{C}$ ), followed by volatilization of

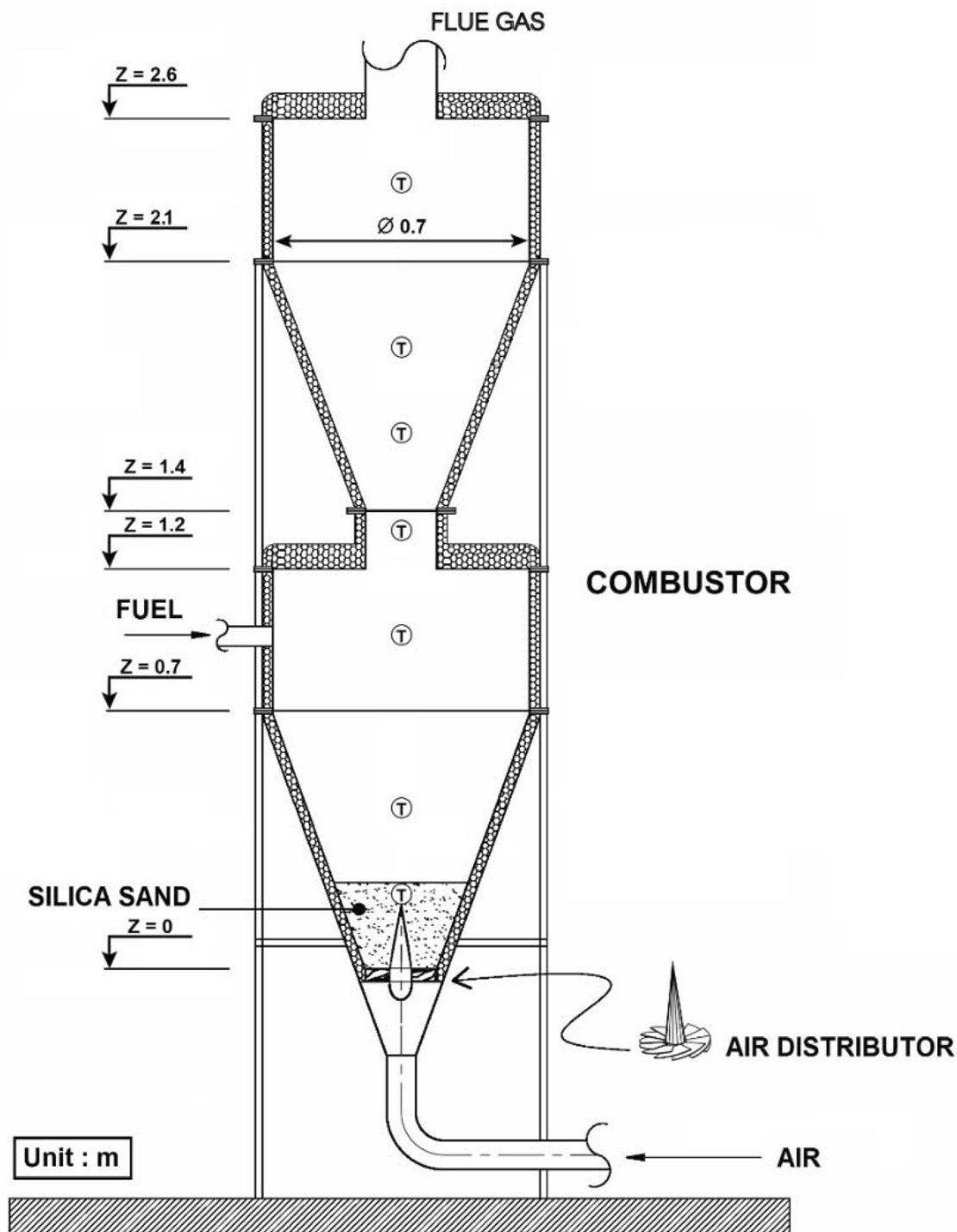


**Fig. 1** Experimental set-up with a twin cyclonic FBC

the cellulose (typically observed at 240–400 °C), and decomposition of lignin at 150–900 °C. These reference temperatures facilitated the characterization of different stages during biomass degradation.

The analysis can be made based on the TG/DTG curves that thermal decomposition of raw biomass feedstock occurred mainly in three sequential stages associated with: (i) biomass dewatering and (ii) devolatilization and volatile oxidation, followed by (iii) char oxidation. Note that the



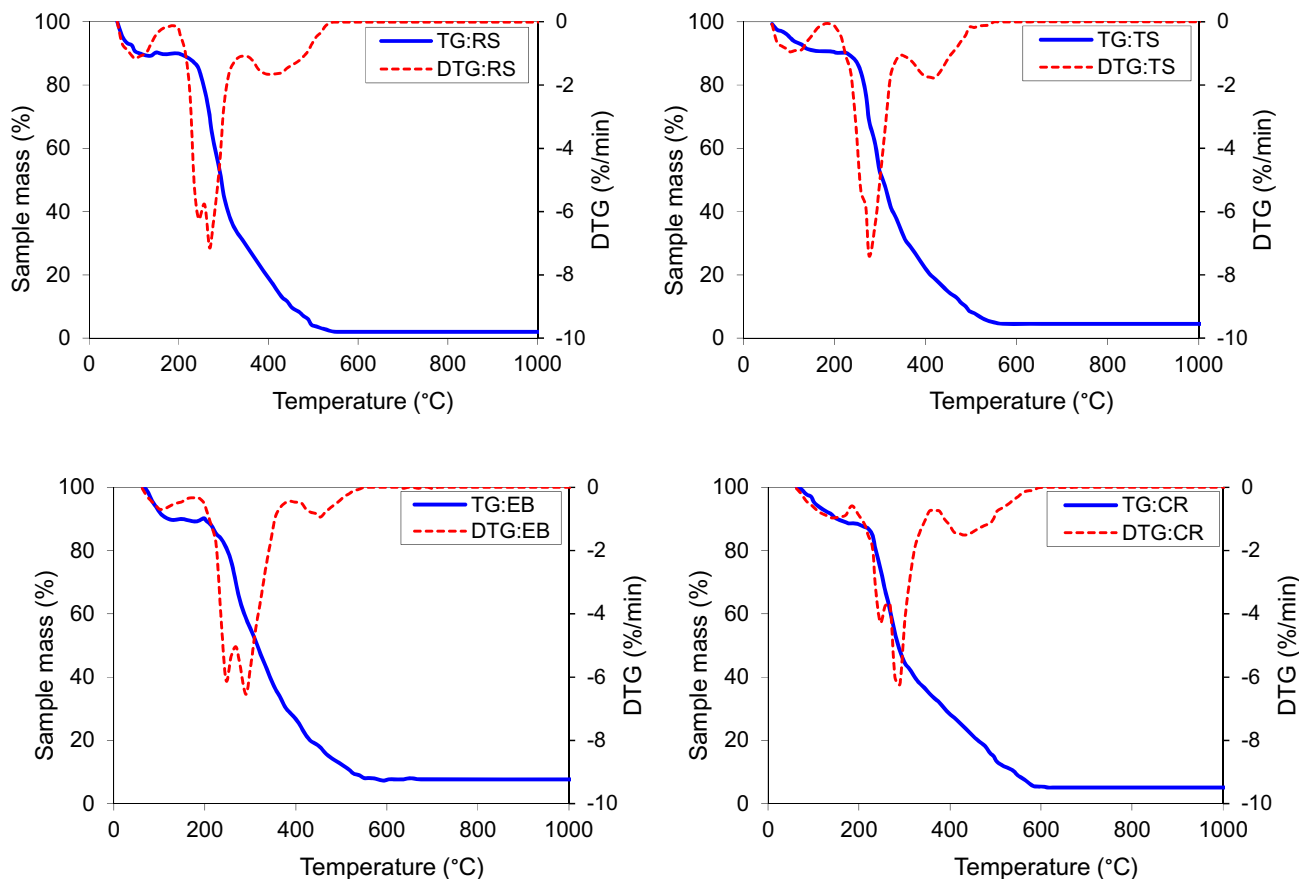


**Fig. 2** The TG/DTG profiles of raw biomasses

effect of biomass dewatering on thermal degradation of the sample was negligible, and it was therefore excluded from this study’s discussion.

Within the temperature range of 180–390 °C, chemical bonds in the biomass began to break, followed by releasing the lightest volatile compounds. Following the temperature regions of major structural compounds mentioned above, this stage was associated with the endothermic volatilization of hemicellulose and cellulose and partial lignin. The rate of mass loss in DTG profiles of RS, EB, and CR exhibited two peaks and corresponding two peak temperatures, related to the volatilization of hemicellulose and cellulose. However, only one peak (attributed to cellulose decomposition) with a small shoulder was observed in the DTG curve for TS, which can be explained by the limited hemicellulose content (1.8 wt.%) in this biomass. As shown in Fig. 2, the biomass degradation in this stage resulted in the sample’s 60–70% weight loss.

At temperatures above 400 °C, a broad reduction of the sample mass was found in the DTG curves, mainly induced by the decomposition of the remaining lignin, accompanied by its conversion into fuel char, and afterward, char oxidation in the analyzer furnace. The remaining material of

the fuel degradation was ash, represented by a constant line in the TG curve.

Figure 3 shows the TG/DTG profiles of the biomass pellets tested under similar operating conditions to those in Fig. 2. The thermal degradation behavior during the devolatilization of pellet samples was similar to that of their original biomasses, exhibiting the same number of peak(s) on the DTG profiles. However, the location of decomposition (peak) temperatures for the pelletized biomasses shifted to higher values compared to the locations for the corresponding raw feedstock, indicating the lower thermal reactivity of the biomass pellets. During the char combustion stage (at temperatures greater than 400 °C), a gradual decrease of the sample mass can be observed over a relatively broad temperature range of DTG profiles with no apparent peaks (except for EBP), pointing to a lower oxidation/combustion rate of biomass pellets in this region. These findings can be explained by the effects of pelletization causing a denser morphology and lowered pore volume, as well as by the pore size of the pellets compared to the as-received materials (Mian et al. 2020; Niu et al. 2017), consequently leading to limited mass and heat diffusion during the devolatilization and char combustion

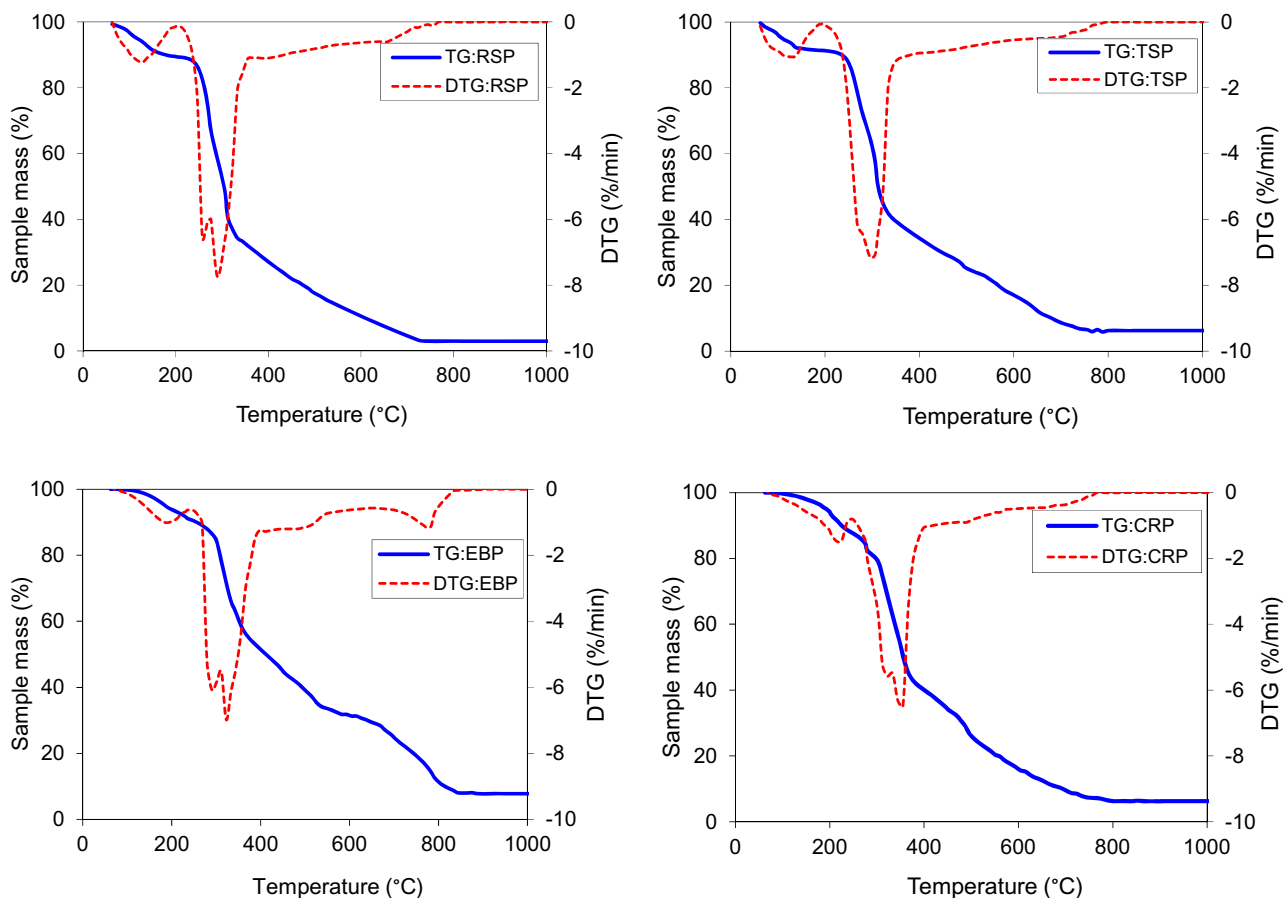


**Fig. 3** The TG/DTG profiles of biomass pellets

stages of pellet combustion in the TGA system. It can be generally concluded that biomass pellets' thermal and combustion reactivity was lower than that of the raw biomasses.

### 3.2 Combustion characteristics of raw and pelletized biomasses

Table 3 summarizes the combustion characteristics ( $T_p$ ,  $T_{ig}$ ,  $T_b$ , and  $S_i$ ) of the raw and pelletized biomasses obtained from the combined analysis of the TG/DTG curves in Figs. 1 and 2, as well as from Eq. (1).

The values of  $T_{p1}$ ,  $T_{p2}$ ,  $T_{p3}$ ,  $T_{ig}$ , and  $T_b$  of the raw biomass samples were 240–246 °C, 268–290 °C, 409–454 °C, 244–258 °C, and 550–593 °C, respectively. These characteristic temperatures of combustion were in agreement with the biomass chemical structure presented in Table 2 and similar to palm oil residues (Idris et al., 2012) and some shell-type biomasses (Kuprianov and Arromdee 2013). From Table 3, the values of  $T_p$  and  $T_{ig}$  for RS were the lowest, while the value of combustion characteristic  $S_i$  was the highest among the other samples, pointing to the

highest thermal and combustion reactivity of this biomass fuel.

As seen in Table 3, the values of  $T_{ig}$ ,  $T_p$ , and  $T_b$  for all pelletized biomasses were higher than those for their corresponding raw biomasses, consistent with the TG/DTG profiles in Figs. 2 and 3. This result implies a lowered reactivity of the biomass pellets. The  $T_{p1}$  and  $T_{p2}$  for the pellets were 257–332 °C and 290–355 °C, respectively. In the case of EBP, the third peak temperature ( $T_{p3}$ ) was found at 800 °C, which was likely to be associated with the thermal instability of lignin and the decomposition of the mineral carbonates contained in EBP at relatively high temperatures (Idris et al. 2010).

The  $T_{ig}$  of the pellets in Table 3 ranged from 259 to 304 °C, 11 to 58 °C higher than the raw biomasses. This result was attributed to a limitation of heat transfer to the dense structure of the pellet samples during the devolatilization stage, leading to delayed ignition of the sample in the analyzer furnace. Note that  $T_{ig}$  values for the biomass pellets found in this study were quite close to those of the shell-type biomass with hard structure reported in other studies (Kuprianov and Arromdee 2013;

**Table 3** Combustion characteristics of raw and pelletized biomasses

Sample	$T_{p1}$ (°C)	$T_{p2}$ (°C)	$T_{p3}$ (°C)	$T_{ig}$ (°C)	$T_b$ (°C)	$S_i \times 10^7$ (% <sup>2</sup> /min <sup>2</sup> °C <sup>3</sup> )
<i>Raw biomass</i>						
RS	240	268	420	244	550	4.50
TS	–	276	409	258	560	3.48
EB	246	290	454	249	581	3.29
CR	243	278	441	246	593	2.77
<i>Biomass pellet</i>						
RSP	257	290	–	259	745	1.83
TSP	–	306	–	269	776	1.69
EBP	290	322	800	296	842	1.41
CRP	332	355	–	304	779	0.93

Ninduangdee et al. 2015). The burnout temperatures for the pellet samples showed a significant increase compared to those for the original biomass, mainly due to the decreased rate of char oxidation, as observed in TG/DTG curves in Fig. 3. Due to the delayed ignition and burnout, the  $S_i$  index values for all biomass pellets in Table 3 were about 2–3 times lower compared to those for the original biomasses. Therefore, the integral combustion characteristics of ignition and burnout for biomass pellets were lower than that of raw biomasses. These findings agreed well with those reported in the literature (Wang et al. 2012; Niu et al. 2017).

Based on the TGA, the selected raw biomasses with a high level of desirable combustion characteristics (taking into account  $T_{ig}$ ,  $T_p$ ,  $T_b$ , and  $S_i$ ) can be used as a fuel in (co-)combustion systems with expected high combustion efficiency. The pellet fuels with a dense structure and high density, consequently, heavy particles, are recommended for use in FBC, ensuring a high residence time and excellent mixing in the reactor (Kaewklum and Kuprianov 2010). Thus, the proposed biomass pellets fired in a fluidized bed at a typical operating temperature (800–900 °C) are expected to have more residence time and good mixing with bed particles in the reactor bottom, leading to a higher burnout rate and high combustion efficiency.

### 3.3 Kinetic parameters

Table 4 summarizes the combustion kinetic parameters ( $E_a$ ,  $A$ , and  $n$ ) of the raw and pelletized biomasses. For accurate fitting of the experimental data, the kinetic parameters of all biomasses were determined for two main stages: (i) devolatilization and volatile oxidation, and (ii) char oxidation, according to the distinct temperature regions of biomass degradation, shown in Figs. 2 and 3.

Activation energy is related to the material's structure and reactivity. The material molecules can only complete the reaction once they have reached the top of the energy barrier corresponding to the  $E_a$  value. This parameter can

be used to measure the reactivity of the fuel; lower  $E_a$  means higher reactivity (Edreis et al. 2014). High  $E_a$  reactions require a high temperature or a longer reaction time (Gil et al. 2010). Besides, this parameter is used for reactor design, simulation, optimization, and control of thermochemical processes (Cai et al. 2014). Data in Table 4 shows that the  $E_a$  values for as-received biomasses during the first (i.e., volatiles combustion) and second stages (i.e., char combustion) of combustion were in the range of 119.1–130.8 kJ/mol and 29.2–34.8 kJ/mol, respectively. The values of  $E_a$  found in this work were in the same ranges as those reported by other researchers. As reported by Vamvuka et al. (2003), the value of  $E_a$  was 90–125 kJ/mol for hemicellulose, 145–285 kJ/mol for cellulose, and 30–39 kJ/mol for lignin. Idris et al. (2012) found that  $E_a$  values for combustion of palm shell, palm fiber, and empty fruit bunch were  $139 \pm 49$ ,  $118 \pm 49$ , and  $105 \pm 56$  kJ/mol, respectively. Kastanaki and Vamvuka (2006) studied combustion kinetics of forest residue, cotton residue, and wood char and calculated  $E_a$  values to be 130, 150, and 145 kJ/mol, respectively.

The  $E_a$  value of RS was the lowest among the other raw biomasses, indicating that this biomass had the highest reactivity, consistent with the abovementioned combustion characteristics in Table 3. As noted in Table 4, the values of  $E_a$  for the volatiles combustion stage were significantly higher than those for the char combustion stage, which was in consistent with other researchers (Wang et al. 2012; Guo and Zhong 2017), who found that the value of  $E_a$  for the release and combustion of volatile compounds stage was higher than that of the char combustion stage. The result indicates that the combustion reaction was controlled by the combustion of volatiles rather than that of char.

From Table 4, the  $E_a$  values of the biomass pellets were greater than those of the as-received biomasses. Mian et al. (2020) observed that the fuel analyses and chemical compositions are the main factors that affect biomass combustion. However, the proximate and ultimate analyses and chemical composition and structure of the as-received

**Table 4** Combustion kinetic parameters of raw and pelletized biomasses

Sample	Temperature range (°C)	Activation energy, $E_a$ (kJ/mol)	Pre-exponential factor, $A$ (1/min)	Reaction order, ( $n$ )	Correlation coefficient, ( $r$ )
<i>Original biomass</i>					
RS	198–334	119.1	$4.36 \times 10^{13}$	4.8	0.983
	344–550	28.5	5.21	1.2	0.983
TS	190–330	130.8	$2.78 \times 10^{15}$	5.0	0.996
	330–560	29.6	4.40	1.3	0.949
EB	186–387	121.0	$1.07 \times 10^{12}$	5.7	0.995
	400–581	29.2	0.79	1.2	0.960
CR	198–365	119.4	$2.95 \times 10^{14}$	7.6	0.984
	376–593	34.8	7.58	1.3	0.912
<i>Biomass pellet</i>					
RSP	214–355	159.3	$2.84 \times 10^{16}$	7.0	0.969
	355–745	47.6	$3.3 \times 10^3$	2.7	0.983
TSP	203–365	165.3	$1.64 \times 10^{17}$	7.5	0.987
	365–776	67.2	$4.9 \times 10^5$	2.8	0.911
EBP	246–409	162.5	$2.05 \times 10^{16}$	10.5	0.984
	409–842	48.6	$1.24 \times 10^3$	2.7	0.912
CRP	240–412	167.8	$2.19 \times 10^{17}$	8.5	0.986
	412–779	47.3	480	1.9	0.955

biomasses and corresponding pellets were similar as seen in Table 2. The compact structure of the biomass pellet caused by pelletization suppressed the mass and heat diffusion and thus resulted in an elevated value of  $E_a$  for the combustion of pellets. The pellets had  $E_a$  values ranging from 159.3 to 167.8 kJ/mol for devolatilization and volatiles combustion stage, and 47.3 to 67.2 kJ/mol for char combustion stage. The increased  $E_a$  values indicated that the biomass pellets required higher energy and temperature, and a longer time for complete combustion. Therefore, biomass pellets' combustion was expected to be more complicated than raw biomasses. Note that the value of  $r$  in Table 4 was relatively high ( $r > 0.91$ ), showing the high correlation of the calculation.

### 3.4 Temperature and $O_2$ concentration in the twin-cyclone FBC

Figure 4 compares the radial profiles of temperature and  $O_2$  in the twin-cyclone FBC at five different levels ( $Z$ ) above the air distributor when firing raw and pelletized biomasses at EA about 50%.

The results in Fig. 4a show important effects of fuel type on the behavior of temperature inside the combustor. The radial temperature for tests with both raw and pelletized biomasses in the lower combustion chamber of the reactor were rather uniform, indicating highly intensive heat-and-mass transfer in the gas–solid flow along the

radial direction. The temperature profiles in the upper combustion chamber exhibited a slightly negative gradient along a radial direction, resulting in a noticeably lower temperature in the peripheral zone of the combustor compared to that at the combustor's center (i.e., at  $r/R = 0$ ). This phenomenon was attributed to heat loss across the combustor walls.

When firing as-received biomasses, the maximum temperature was observed in the vicinity of fuel injection (at  $Z = 0.95$  m). Based on the TGA discussed above, substantial gaseous volatiles were generated during raw biomass combustion at temperatures of 180–390 °C. However, the temperatures inside the combustor during operation were 800–900 °C, substantially higher than the devolatilization temperature of biomass particles. Thus, the endothermic drying and devolatilization of biomass occurred rapidly once the as-received biomass was introduced into the combustor by the fuel feeder. Meanwhile, fine and light char particles were generated in the combustor during the combustion of raw biomasses, especially when firing dust-like biomasses (i.e., RS and TS). Significant portions of these fine char particles were carried out from the conical section and burned in the cylindrical section of the lower combustion chamber. It can be observed in Fig. 4a that temperatures inside the combustor decreased with combustor height because of the effect of heat loss across the combustor wall. At  $Z > 0.95$  m, temperatures at all points inside the combustor burning raw

biomasses were relatively higher than those for burning biomass pellets. This result can be explained by the carry-over of relatively light biomass/char from the lower combustion chamber into the upper chamber, contributing to a greater heat release in the higher combustor levels.

Despite the lower thermal and combustion reactivity of all biomass pellets compared to that of the original biomasses, as revealed by the TGA study, the bed temperatures (at  $Z = 0.45$  m) when firing all pelletized biomasses were higher than burning the as-received feedstock at the same EA. At the fuel feeding point, the pellet particles released volatiles rapidly, however, at a lower rate than the

as-received biomasses according to the thermal decomposition found in the TGA. Due to the dense structure of the pellets, larger and heavier char particles were formed in the combustor that fell and penetrated the fluidized bed. These char particles had a longer residence time in the combustor bottom, leading to greater combustion intensity in this dense bed zone. A large amount of combustion heat was released in the bed zone, resulting in the maximum temperature in the conical section of the lower combustion chamber (at  $Z = 0.45$  m). Similar behaviors have been reported in the pioneering study (Ninduangdee and Kuprianov 2018).

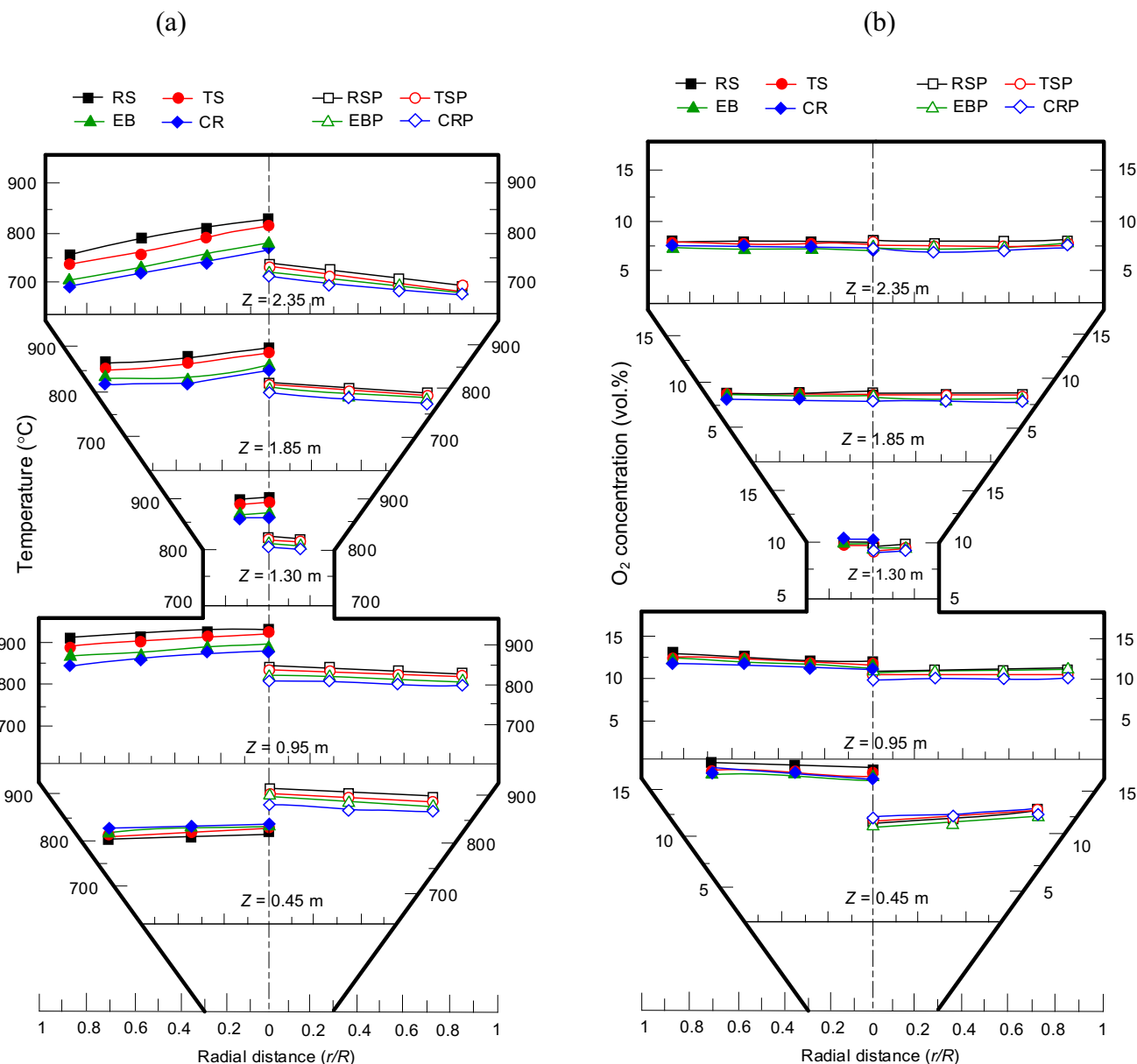


**Fig. 4** Distribution of **a** temperature and **b**  $O_2$  in radial direction at different levels inside the twin-cyclone FBC when firing raw and pelletized biomasses at excess air of about 50%



As shown in Fig. 4a, the temperature at the combustor bottom when firing RSP was the highest compared to the other pellet fuels. This fact can be explained by this fuel's highest thermal and combustion reactivity. On the other hand, CRP, with the lowest thermal and combustion reactivity, had the lowest bed temperature among the selected fuels.

As shown in Fig. 4b, the radial  $O_2$  concentration profiles were relatively uniform. It can be explained by the intensive gas–solid and gas–gas mixing in the radial direction and by the uniform distribution of airflow across the bed, the latter ensured by the unique design of the twin-cyclone FBC providing a swirling gas–solid bed.

The concentrations of  $O_2$  in the combustor at  $Z = 0.45$  m for the test runs with biomass pellets were substantially lower than those for burning raw biomasses. This result indicated that a more significant proportion of  $O_2$  was consumed for the oxidization of CO,  $C_xH_y$ , char-C, and other combustible species released from the pellets in the fluidized bed (i.e., in a conical section of the lower combustion chamber), resulting in a greater fuel burnout in this region. Meanwhile,  $O_2$  consumption was significant in the cylindrical part of the lower combustion chamber (at  $Z = 0.95$  m) and the connecting pipe (at  $Z = 1.30$  m) when firing raw biomasses. This phenomenon can be explained by the oxidation of fine char particles carried over from the dense bed zone (i.e., conical section). In the upper combustion chamber (at  $Z > 1.30$  m), the rate of  $O_2$  consumption (and, accordingly, biomass oxidation) was substantially lower than in the lower chamber. At the reactor top,  $O_2$  correlated with the specified percentage of EA (i.e., at about 50%).

### 3.5 Emissions of CO, $C_xH_y$ , and NO

Figure 5 depicts the CO,  $C_xH_y$ , and NO emissions from the twin-cyclone FBC (all on a dry gas basis and at 6%  $O_2$ ) tested with raw and pelletized biomasses at an identical heat input to the combustor for varying values of EA from about 40 to 60%. As shown in Fig. 5, the major gaseous pollutants were significantly influenced by the fuel properties and the amount of EA.

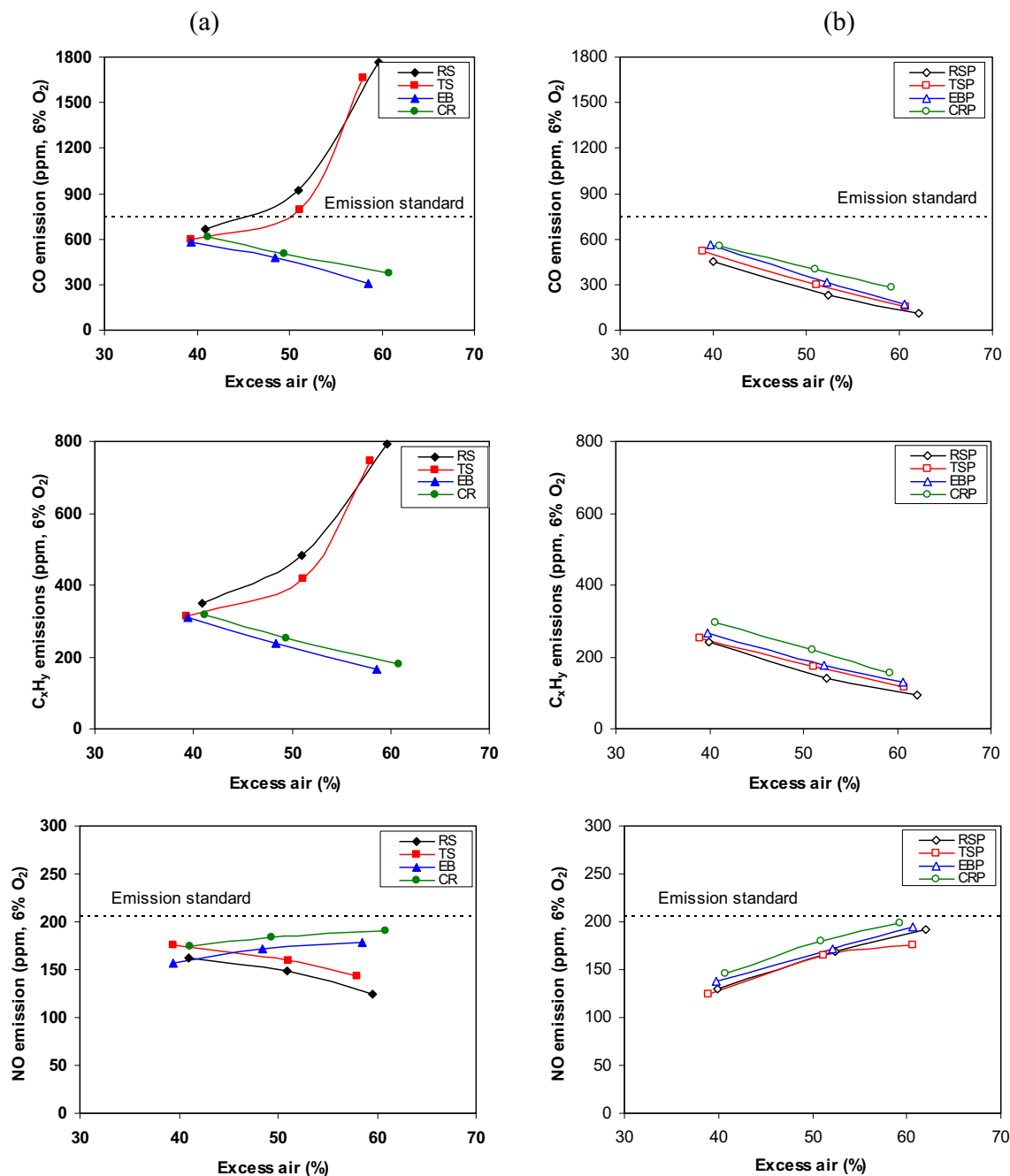
For most fuel options, except RS and TS, the CO and  $C_xH_y$  emissions can be mitigated by increasing EA, which was attributed mainly to the increased oxidation rates of CO and  $C_xH_y$  to  $CO_2$  by excessive  $O_2$ . In the comparisons shown in Fig. 5a and b with similar amounts of EA, the CO and  $C_xH_y$  emissions for testing biomass pellets were noticeably lower than for raw biomass, despite the lower thermal and combustion reactivity of these fuels. During combustion of biomass pellets, oxidation of the volatile CO and  $C_xH_y$ , as well as of fuel chars, occurred substantially in the fluidized bed, as indicated by the temperature profile in

Fig. 4. The oxidation of CO in chemical reactions involved  $O_2$  and OH, whereas the  $C_xH_y$  oxidation occurred via two groups of secondary reactions: (i) breakdown of  $C_xH_y$  to CO, and afterward (ii) oxidation of CO to  $CO_2$  (Turns 2006). The above-mentioned higher residence time of the fuel in the fluidized bed and the higher bed temperature enhanced the reactions for CO and  $C_xH_y$  oxidations. As a result, higher burnout (i.e., lower CO and  $C_xH_y$  emissions) can be achieved when burning biomass pellets. It can be further noticed from Fig. 5b that burning more highly reactive pellet fuels resulted in diminished CO and  $C_xH_y$  emissions from the combustor, which can be explained by the higher burnout rate of the fuel inside the reactor particularly in the bed region.

When firing RS and TS, the EA exhibited reverse effects on the CO and  $C_xH_y$  emissions. An increased EA led to an increase in these emissions, with this effect more significant when increasing amounts of EA to approximately 50–60%. This behavior can be explained by the lower burn rate of these fuels in the reactor, particularly in the lower combustion chamber, due to the carry-over mentioned above of fuel/char and lower residence time. The CO and  $C_xH_y$  emissions from testing with EB and CR exhibited similar effects of EA as for the tests with biomass pellets, however, to different extents.

Note that the CO emission levels from all the tests with biomass pellets were lower than the emissions limit in Thailand (740 ppm, at 6%  $O_2$  on a dry gas basis (PCD 2013)), whereas the emission levels were unacceptable when firing dust-like biomasses (i.e., RS and TS) at EA above 50%. Therefore, the combustor fired with RS and TS should be operated with EA lower than 50% to control CO emission within the above-mentioned emission standard.

Unlike CO and  $C_xH_y$  emissions, the NO emission from the twin-cyclone FBC can be reduced by decreasing EA, except when firing RS and TS showing the opposite effects of EA on this type of emission. During biomass combustion, NO emission can be reduced via heterogeneous reduction of NO by CO and light hydrocarbons on the surface of various catalysts (char, ash, and bed material particles), as well as (ii) homogeneous reactions of NO with  $C_xH_y$  (Winter et al. 1999). Due to the high CO and  $C_xH_y$  when testing at low EA, the contribution of CO,  $C_xH_y$ , and char particles to NO emission reduction was significant. NO was reduced by the above-mentioned catalytic reaction with CO and some hydrocarbons on the char surface and homogeneous with  $C_xH_y$ . Because of the high combustion intensity of the twin-cyclone FBC, the reactions for NO reduction can be enhanced in the fluidized bed region of the lower combustion chamber, particularly when burning pellet fuels. As shown in Fig. 5, burning CR and CRP with elevated fuel N content generated the highest NO



**Fig. 5** Emissions of CO, C<sub>x</sub>H<sub>y</sub> (as CH<sub>4</sub>), and NO from the twin-cyclone FBC when firing **a** raw and **b** pelletized biomasses at variable EA

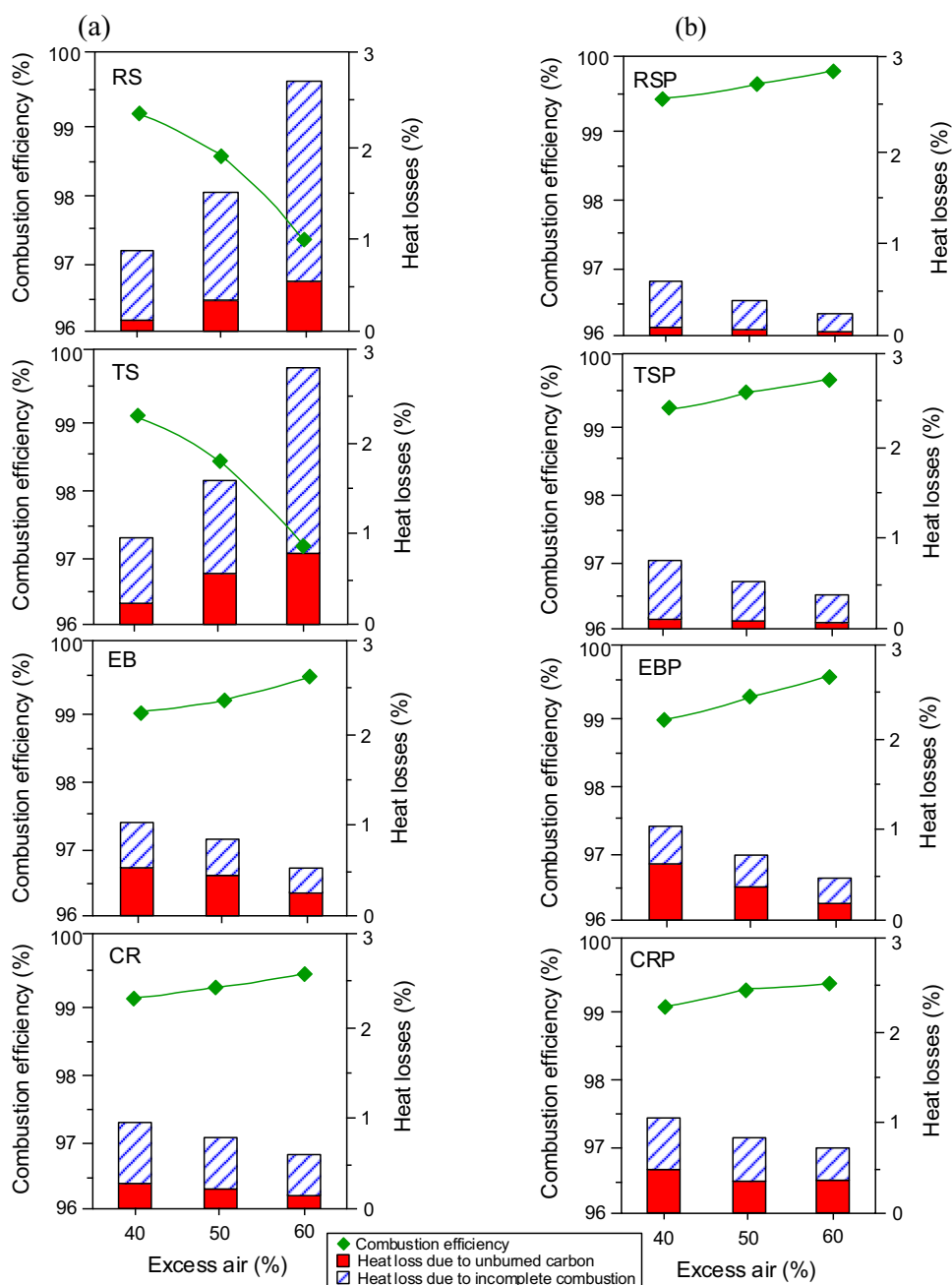
emission, following the fuel-NO formation mechanism (Winter et al. 1999). When burning RS and TS with higher EA, the NO emission diminished mainly due to higher levels of CO and C<sub>x</sub>H<sub>y</sub> concentration in the combustor, attributed to the above-mentioned catalytic reduction of NO to N<sub>2</sub>. Note that the NO emission from all the tests was relatively low, showing values below Thailand’s emissions standards (214 ppm, at 6% O<sub>2</sub> on a dry gas basis (PCD 2013)).

### 3.6 Combustion efficiency

The combustion-related heat losses (due to unburned carbon and incomplete combustion) and the combustion efficiency of the twin-cyclone FBC when firing raw and pelletized biomasses at variable EA are depicted in Fig. 6.

The fuel type and EA substantially affected the heat losses and combustion efficiency of the combustor. Despite the higher thermal and combustion reactivity of RS and TS, the combustion efficiency of the combustor when firing

**Fig. 6** Combustion-related heat losses and combustion efficiency (LHV%) of the twin-cyclone FBC when firing **a** raw and **b** pelletized biomasses at variable amounts of excess air (EA)



these fuels was lower than other fuel options, strengthened by the amount of EA. Both types of heat loss increased substantially with an increased amount of EA, following the previously discussed carry-over of fuel particles and the behavior of CO and  $C_xH_y$  emissions.

The combustion efficiency of the combustor tested with the other two raw biomasses and pellet fuels exhibited an improvement when operated at a higher value of EA. Both heat losses decreased significantly with an increasing amount of EA within the specified range. From Fig. 6a and b, the heat loss owing to incomplete combustion in all tests with pellet fuels was lower than those for raw biomasses,

following the characteristics of CO and  $C_xH_y$  emissions, as depicted in Fig. 5. This result indicated a higher burnout and more complete combustion of the pelletized fuels, owing to fuel char particles' more excellent residence time in a fluidized bed and a higher bed temperature. For the range of EA, the combustor operated at high combustion efficiency: 97.4–99.5% for firing as-received biomasses and 99.0–99.8% for firing biomass pellets.

Based on the combustion and emission characteristics discussed above, the amount of EA should be optimized to achieve the highest performance of the combustor. Compared to CO and  $C_xH_y$ , NO is a more harmful gas that

**Table 5** Comparison of gaseous emissions and combustion efficiency among different types of FBCs when firing various biomasses at excess air about 40%

Biomass fuel	LHV (kJ/kg)	Heat input (kW)	Combustor/furnace	EA (%)	Combustion intensity in main combustion zone <sup>a</sup> (kW/m <sup>3</sup> )	Emissions (ppm) <sup>b</sup>			Combustion efficiency (%)	References
						CO	C <sub>x</sub> H <sub>y</sub>	NO		
Cotton stalk	17,531	170	Bubbling FBC	36 <sup>c</sup>	n/a	190	n/a	n/a	99.9 <sup>f</sup>	Sun et al. (2008)
Oil palm shell	19,427	265	Swirling FBC	36	n/a	258	n/a	254	99.7 <sup>g</sup>	Batcha et al. (2020)
Rice husk	14,980	100	Cyclonic FBC	67	950	400	n/a	350	98.0 <sup>g</sup>	Madhiyanon et al. (2006)
Pelletized peanut shells	16,741	150	Vortexing FBC	50 <sup>d</sup>	330	53	n/a	160	98.0 <sup>h</sup>	Duan et al. (2014)
Sun flower shells	18,030	225	Conical FBC	41	870	494	96	166	99.3 <sup>h</sup>	Sirisomboon and Charernporn (2017)
Rice husk	13,300	100	Twin-cyclone FBC	40	813	520	260	160	91.1 <sup>g</sup>	Ninduangdee et al. (2020)
RS	16,200	120	Twin-cyclone FBC	41 <sup>e</sup>	975	666	350	162	99.1 <sup>h</sup>	Current study
TS	16,600	120	Twin-cyclone FBC	39 <sup>e</sup>	975	593	315	176	99.1 <sup>h</sup>	Current study
EB	13,260	120	Twin-cyclone FBC	39 <sup>e</sup>	975	580	309	157	99.0 <sup>h</sup>	Current study
CR	15,560	120	Twin-cyclone FBC	41 <sup>e</sup>	975	613	318	174	99.1 <sup>h</sup>	Current study
RSP	17,500	120	Twin-cyclone FBC	40 <sup>e</sup>	975	450	240	130	99.4 <sup>h</sup>	Current study
TSP	18,180	120	Twin-cyclone FBC	39 <sup>e</sup>	975	517	254	124	99.3 <sup>h</sup>	Current study
EBP	14,700	120	Twin-cyclone FBC	40 <sup>e</sup>	975	565	265	138	99.0 <sup>h</sup>	Current study
CRP	17,050	120	Twin-cyclone FBC	41 <sup>e</sup>	975	555	295	146	99.0 <sup>h</sup>	Current study

<sup>a</sup>Estimated by the authors of this study

<sup>b</sup>On a dry basis and at 6% O<sub>2</sub>

<sup>c</sup>Using air staging: <sup>d</sup>Using flue gas recirculation

<sup>e</sup>Optimal excess air

<sup>f</sup>Taking in to accounting effects of CO only

<sup>g</sup>Taking in to accounting effects of CO and unburned carbon in fly ash

<sup>h</sup>Taking in to accounting effects of CO, C<sub>x</sub>H<sub>y</sub> and unburned carbon in fly ash

adversely impacts the environment and human health. Therefore, it is suggested to operate the combustor at a minimum possible EA to minimize NO emission and heat loss with flue gas, while ensuring CO emission below the emission standard mentioned above. Based on such criteria, EA of about 40% can be regarded as the optimal option for firing all fuel options in the twin-cyclone FBC. Under the optimum EA, the twin-cyclone FBC can operate with more than 99% combustion efficiency and control the CO and NO emissions below the emission standard of Thailand. The C<sub>x</sub>H<sub>y</sub> emission is also maintained at low level.

Table 5 compares the CO, C<sub>x</sub>H<sub>y</sub>, and NO emissions and combustion efficiency of the twin-cyclone FBC fired with the proposed biomasses and other pilot-scale FBCs burning

various biomasses for selected EA. Table 5 also includes important thermal characteristics of the combustor, including heat input and estimated combustion intensity in the main combustion zone. Based on the above-mentioned optimal EA for firing the selected fuel options, the cases have been selected for EA of about 40% for comparability of the results. As can be seen in Table 5, all FBCs operate at high combustion performance and efficiency (about 99%). The combustion efficiency seems more accurate when the effects of unburned carbon (in fly ash) and CO and C<sub>x</sub>H<sub>y</sub> in exhaust gas leaving the combustor are considered. Compared to other FBCs, the twin-cyclone FBC fired with the proposed biomasses emitted a relatively higher CO emission but lower NO emission. Table 5 shows

that the NO emission from the optimally-operated twin-cyclone FBC firing pellet fuel was substantially lower than in other case studies. This fact can be resulted from high ( $975 \text{ kW/m}^3$ ) combustion intensity in the lower combustor's chamber compared to other FBCs. Considering the above characteristics of combustors shown in Table 5, the twin-cyclone FBC fired with biomass pellets has an advantage for high combustion efficiency and NO reduction.

Based on the findings from the combustion experiment in the twin-cyclone FBC, the combustion property of the as-received biomasses (particularly the dusk-like fuels) was enhanced by pelletization. Although this process led to diminishing thermal and combustion reactivity of the proposed fuel options, the physical combustion property of these biomasses significantly improved.

### 3.7 Practical applications and future work

The main significance of this study is information on the combustion of pelletized biomasses, including RSP, TSP, EBP, and CRP, that could be used as a fuel in heat and power generation. This information is essential for the large-scale combustion process. The characteristic combustion temperatures and activation energy found in this work can be used to analyze thermal behaviors, which are very helpful for efficient design, optimization, and control of combustion systems. Based on the combustion and emission characteristics of the pilot-scale twin-cyclone FBC, the proposed biomass pellets can be recommended for steam production of fluidized-bed boilers. The as-received biomass can also be co-fired with coal or other high-quality biomasses. In the future, further study on long-term combustion is essential to ensure a safe and reliable combustor operation. Although no evidence of bed agglomeration was observed during the combustion experiments, a detailed investigation of bed material characteristics is needed to assess this problem's tendency, especially when firing high-ash biomass (i.e., EBP and CRP). Furthermore, a co-combustion study of the proposed biomass pellets with some unconventional biomasses is needed to be conducted to extend the information on the use of biomass for energy production.

## 4 Conclusions

Combustion characteristics of raw and pelletized biomasses from rubberwood sawdust, teak sawdust, eucalyptus bark, and cassava rhizomes have been investigated in a thermogravimetric system and a pilot-scale twin-cyclone fluidized-bed combustor. Combustion of these biomasses can be divided into three stages: (i) biomass dewatering

and (ii) devolatilization and volatile oxidation, followed by (iii) char oxidation. Pelletized biomasses have lower combustion reactivity than raw biomass, as higher ignition, peak, and burnout temperatures, and lower comprehensive performance index values. The activation energies of raw biomasses and pellets for devolatilization and volatiles combustion stage are  $119.1\text{--}130.8 \text{ kJ/mol}$  and  $159.3\text{--}167.8 \text{ kJ/mol}$ , whereas for char combustion are  $29.2\text{--}34.8 \text{ kJ/mol}$  and  $47.3\text{--}67.2 \text{ kJ/mol}$ , respectively. Fuel properties and excess air significantly impact the combustor's combustion characteristics. The biomass pellets have higher residence time and excellent mixing with bed particles in a fluidized bed, leading to more significant combustion intensity in the bed region. This result contributes to higher fuel burnout, as lower CO and  $\text{C}_x\text{H}_y$  emissions. When raw biomasses are fired with high excess air, the carry-over of light char particles causes elevated CO and  $\text{C}_x\text{H}_y$  emissions and combustion heat losses, consequently lowering combustion efficiency. The combustor fired with pellet fuels emits relatively low NO emission due to the high combustion intensity in the fluidized bed. Excess air of about 40% is optimal for firing the selected biomass in this combustor, ensuring above 99% combustion efficiency and low emission characteristics. Therefore, the proposed biomasses in both forms have a high level of desirable combustion characteristics, which can be used as a fuel in practical (co-)combustion systems with expected high combustion efficiency and low emissions.

### Appendix A: Models for determining combustion-related heat losses and combustion efficiency

The heat-loss method (Basu et al., 2000) was used to quantify combustion efficiency of the twin-cyclone FBC when firing the proposed biomass.

The heat loss owing to unburned carbon,  $q_{uc}$  (%LHV) was predicted by using the measured fraction of unburned carbon in fly ash carried over from the combustor ( $C_{fa}$ , wt%) determined using a "Perkin Elmer PE2400 Series II" CHNS/O elemental analyzer, the fuel-ash content (A, wt%, on as-received basis), and the fuel lower heating value (LHV, kJ/kg, on an as-received basis) as:

$$q_{uc} = \frac{32,866}{\text{LHV}} \left( \frac{C_{fa}}{100 - C_{fa}} \right) A \quad (\text{A1})$$

The heat loss owing to incomplete combustion,  $q_{ic}$  (%LHV), was quantified using the above-calculated  $q_{uc}$  and CO and  $\text{C}_x\text{H}_y$  (as  $\text{CH}_4$ ) emissions (in ppm, on a dry gas basis and at 6%  $\text{O}_2$ ) as:



$$q_{ic} = (126.4 \text{ CO} + 358.2 \text{ CH}_4)_{@6\%O_2} 10^{-4} V_{dg@6\%O_2} \frac{(100 - q_{uc})}{LHV} \quad (\text{A2})$$

where  $V_{dg@6\% O_2}$  is calculated according to Kuprianov and Arromdee (2013) using the fuel composition on “as-received” basis. The combustion efficiency of the fluidized-bed combustors,  $\eta_c$  (%LHV), was then determined as:

$$\eta_c = 100 - (q_{uc} + q_{ic}) \quad (\text{A3})$$

**Acknowledgements** The authors would like to sincerely acknowledge the financial support received from Thailand Science Research and Innovation (TSRI), Phetchaburi Rajabhat University, and the Department of Mechanical Engineering, Faculty of Engineering and Industrial Technology, Silpakorn University.

**Credit authorship contribution statement** PA: Designed and performed experiments, and undertook systematic review, statistical analysis, original drafting, and revision writing. PN: Undertook conceptualization, performed experiments, undertook data curation interpretation, writing, reviewing, revision writing and editing.

#### Declarations

**Conflict of interest** The authors declare that they have no known competing financial interests or personal relationships that could have appeared to influence the work reported in this paper.

#### References

- Basu P, Kefa C, Jestin L (2000) Boilers and burners: design and theory. Springer, New York
- Batcha MFM, Othaman MF, Sabudin S, Mohammed AN, Abdullah MK, Ali MFM (2020) Combustion and emission of pelletized empty fruit bunch and oil palm shell in a swirling fluidized bed combustor. *Biomass Convers Biorefin* 10(3):755–763. <https://doi.org/10.1007/s13399-020-00903-x>
- Cai J, Wu W, Liu R (2014) An overview of distributed activation energy model and its application in the pyrolysis of lignocellulosic biomass. *Renew Sust Energ Rev* 36:236–246. <https://doi.org/10.1016/j.rser.2014.04.052>
- Chirone R, Salatino P, Scala F, Solimene R, Urciuolo M (2008) Fluidized bed combustion of pelletized biomass and waste-derived fuels. *Combust Flame* 155:21–36. <https://doi.org/10.1016/j.combustflame.2008.05.013>
- Coats AW, Redfern JP (1964) Kinetic parameters from thermogravimetric data. *Nature* 201(4914):68–69. <https://doi.org/10.1038/201068a0>
- DEDE (2020) Department of Alternative Energy Development and Efficiency, Thailand Alternative Energy Situation 2020. <https://www.dede.go.th/download/stat63/Thailand%20Alternative%20Energy%20Situation%202020.pdf> Accessed 10 Oct 2021
- Duan F, Zhang JP, Chyang CS, Wang YJ, Tso J (2014) Combustion of crushed and pelletized peanut shells in a pilot-scale fluidized-bed combustor with flue gas recirculation. *Fuel Process Technol* 128:28–35. <https://doi.org/10.1016/j.fuproc.2014.06.022>
- Edreis EMA, Luo G, Yao H (2014) Investigations of the structure and thermal kinetic analysis of sugarcane bagasse char during non-isothermal CO<sub>2</sub> gasification. *Anal Appl Pyrolysis* 107:107–115. <https://doi.org/10.1016/j.jaap.2014.02.010>
- Gil MV, Casal D, Pevida C, Pis JJ, Rubiera F (2010) Thermal behaviour and kinetics of coal/biomass blends during co-combustion. *Bioresour Technol* 101(14):5601–5608. <https://doi.org/10.1016/j.biortech.2010.02.008>
- Guo F, Zhong Z (2017) Experimental studies on combustion of composite biomass pellets in fluidized bed. *Sci Total Environ* 599–600:926–933. <https://doi.org/10.1016/j.scitotenv.2017.05.026>
- Haykiri-Acma H, Yaman S, Kucukbayrak S (2010) Comparison of the thermal reactivities of isolated lignin and holocellulose during pyrolysis. *Fuel Process Technol* 91:759–764. <https://doi.org/10.1016/j.fuproc.2010.02.009>
- Idris SS, Rahman NA, Ismail AB, Rashid ZA, Aris MJ (2010) Investigation on thermochemical behaviour of low rank Malaysian coal, oil palm biomass and their blends during pyrolysis via thermogravimetric analysis (TGA). *Bioresour Technol* 101(12):4584–4592. <https://doi.org/10.1016/j.biortech.2010.01.059>
- Idris SS, Rahman NA, Ismail K (2012) Combustion characteristics of Malaysian oil palm biomass, sub-bituminous coal and their respective blends via thermogravimetric analysis (TGA). *Bioresour Technol* 123:581–591. <https://doi.org/10.1016/j.biortech.2012.07.065>
- Jiang L, Yuan X, Li H, Xiao Z, Liang J, Wang H, Wu Z, Chen X, Zeng G (2015) Pyrolysis and combustion kinetics of sludge-camphor pellet thermal decomposition using thermogravimetric analysis. *Energ Convers Manage* 106:282–289. <https://doi.org/10.1016/j.enconman.2015.09.046>
- Kaewklum R, Kuprianov VI (2010) Experimental studies on a novel swirling fluidized-bed combustor using an annular spiral air distributor. *Fuel* 89(1):43–52. <https://doi.org/10.1016/j.fuel.2009.07.027>
- Kastanaki E, Vamvuka D (2006) A comparative reactivity and kinetic study on the combustion of coal–biomass char blends. *Fuel* 85(9):1186–1193. <https://doi.org/10.1016/j.fuel.2005.11.004>
- Kongto P, Palamanit A, Ninduangdee P, Singh Y, Chanakaewsomboon I, Hayat A, Wae-hayee M (2022) Intensive exploration of the fuel characteristics of biomass and biochar from oil palm trunk and oil palm fronds for supporting increasing demand of solid biofuels in Thailand. *Energy Rep* 8:5640–5652. <https://doi.org/10.1016/j.egy.2022.04.033>
- Kuprianov VI, Arromdee P (2013) Combustion of peanut and tamarind shells in a conical fluidized-bed combustor: a comparative study. *Bioresour Technol* 140:199–210. <https://doi.org/10.1016/j.biortech.2013.04.086>
- Madhiyanon T, Lapirattanakun A, Sathitruangsak P, Soponronnarit S (2006) A novel cyclonic fluidized-bed combustor ( $\psi$ -FBC): combustion and thermal efficiency, temperature distributions, combustion intensity, and emission of pollutants. *Combust Flame* 146(1):232–425. <https://doi.org/10.1016/j.combustflame.2006.03.008>
- Magdziarz A, Wilk M (2013) Thermal characteristics of the combustion process of biomass and sewage sludge. *J Therm Anal Calorim* 114:519–529. <https://doi.org/10.1007/s10973-012-2933-y>
- Malico I, Pereira RN, Gonçalves AC, Sousa AMO (2019) Current status and future perspectives for energy production from solid biomass in the European industry. *Renew Sust Energ Rev* 112:960–977. <https://doi.org/10.1016/j.rser.2019.06.022>
- Martsri A, Yodpijit N, Jongprasithporn M, Junsupasen S (2021) Energy, economic and environmental (3E) analysis for sustainable development: a case study of a 9.9 MW biomass power plant in Thailand. *Appl Sci Eng Prog* 14(3):378–386. <https://doi.org/10.14416/j.asep.2020.07.002>

- Mian I, Li X, Dacres OD, Wang J, Wei B, Jian Y, Zhong M, Liu J, Ma F, Rahman N (2020) Combustion kinetics and mechanism of biomass pellet. *Energy* 205:117909. <https://doi.org/10.1016/j.energy.2020.117909>
- Ninduangdee P, Kuprianov VI (2014) Combustion of palm kernel shell in a fluidized bed: optimization of biomass particle size and operating conditions. *Eng Convers Manage* 85:800–808. <https://doi.org/10.1016/j.enconman.2014.01.054>
- Ninduangdee P, Kuprianov VI (2018) Fluidized bed co-combustion of rice husk pellets and moisturized rice husk: the effects of co-combustion methods on gaseous emissions. *Biomass Bioenergy* 112:73–84. <https://doi.org/10.1016/j.biombioe.2018.02.016>
- Ninduangdee P, Kuprianov VI, Cha EY, Kaewrath R, Youngyuen P, Athawethworawuth W (2015) Thermogravimetric studies of oil palm empty fruit bunch and palm kernel shell: TG/DTG analysis and modeling. *Energy Procedia* 79:453–458. <https://doi.org/10.1016/j.egypro.2015.11.518>
- Ninduangdee P, Arromdee P, Se C, Kuprianov VI (2020) Effects of (co-)combustion techniques and operating conditions on the performance and NO emission reduction in a biomass-fueled twin-cyclone fluidized-bed combustor. *Waste Biomass Valori* 11(10):5375–5391. <https://doi.org/10.1007/s12649-020-01124-z>
- Niu S, Chen M, Li Y, Xue F (2016) Evaluation on the oxy-fuel combustion behavior of dried sewage sludge. *Fuel* 178:129–138. <https://doi.org/10.1016/j.fuel.2016.03.053>
- Niu S, Chen M, Li Y, Lu T (2017) Combustion characteristics of municipal sewage sludge with different initial moisture contents. *J Therm Anal Calorim* 129(2):1189–1199. <https://doi.org/10.1007/s10973-017-6262-z>
- PCD (2013) Pollution control department, ministry of natural resources and environment, Thailand, Air pollution standards for industrial sources. [http://www.pcd.go.th/info\\_serv/reg\\_std\\_airsnd03.html](http://www.pcd.go.th/info_serv/reg_std_airsnd03.html). Accessed 26 Jan 2022
- Permchart W, Kuprianov VI (2004) Emission performance and combustion efficiency of a conical fluidized-bed combustor firing various biomass fuels. *Bioresour Technol* 92:83–91. <https://doi.org/10.1016/j.biortech.2003.07.005>
- Quan LM, Kamyab H, Yuzir A, Ashokkumar V, Hosseini SE, Balasubramanian B, Kirpichnikova I (2022) Review of the application of gasification and combustion technology and waste-to-energy technologies in sewage sludge treatment. *Fuel* 316:123199. <https://doi.org/10.1016/j.fuel.2022.123199>
- Rokni E, Ren X, Panahi A, Levendis YA (2018) Emissions of SO<sub>2</sub>, NO<sub>x</sub>, CO<sub>2</sub>, and HCl from Co-firing of coals with raw and torrefied biomass fuels. *Fuel* 211:363–374. <https://doi.org/10.1016/j.fuel.2017.09.049>
- Saikia M, Ali AA, Borah RC, Bezbarua MS, Saikia BK, Saikia N (2018) Effects of biomass types on the co-pyrolysis behaviour of a sub-bituminous high-sulphur coal. *Energy Ecol Environ* 3(5):251–265. <https://doi.org/10.1007/s40974-018-0097-8>
- Shimizu T, Han J, Choi S, Kim L, Kim H (2006) Fluidized-bed combustion characteristics of cedar pellets by using an alternative bed material. *Energy Fuels* 20:2737–2742. <https://doi.org/10.1021/ef0601723>
- Sirisomboon K, Chareernporn P (2017) Effects of air staging on emission characteristics in a conical fluidized-bed combustor firing with sunflower shells. *J Energy Inst* 90(2):316–323. <https://doi.org/10.1016/j.joei.2015.12.001>
- Sun Z, Jin B, Zhang M, Liu R, Zhang Y (2008) Experimental studies on cotton stalk combustion in a fluidized bed. *Energy* 33:1224–1232. <https://doi.org/10.1016/j.energy.2008.04.002>
- Tumuluru JS (2018) Effect of pellet die diameter on density and durability of pellets made from high moisture woody and herbaceous biomass. *Carbon Resour Convers* 1(1):44–54. <https://doi.org/10.1016/j.crcon.2018.06.002>
- Turns S (2006) An introduction to combustion. McGraw-Hill, Boston
- Vamvuka D, Kakaras E, Kastanaki E, Grammelis P (2003) Pyrolysis characteristics and kinetics of biomass residuals mixtures with lignite. *Fuel* 82(15):1949–1960. [https://doi.org/10.1016/S0016-2361\(03\)00153-4](https://doi.org/10.1016/S0016-2361(03)00153-4)
- Van Soest PJ, Robertson JB, Lewis BA (1991) Methods for dietary fiber, neutral detergent fiber, and nonstarch polysaccharides in relation to animal nutrition. *J Dairy Sci* 74(10):3583–3597. [https://doi.org/10.3168/jds.S0022-0302\(91\)78551-2](https://doi.org/10.3168/jds.S0022-0302(91)78551-2)
- Wang X, Si J, Tan H, Niu Y, Xu C, Xu T (2012) Kinetics investigation on the combustion of waste capsicum stalks in Western China using thermogravimetric analysis. *J Therm Anal Calorim* 109(1):403–412. <https://doi.org/10.1007/s10973-011-1556-z>
- Werther J, Saenger M, Hartge EU, Ogada T, Otara S (2000) Combustion of agricultural residues. *Prog Energy Combust Sci* 26:1–27. [https://doi.org/10.1016/S0360-1285\(99\)00005-2](https://doi.org/10.1016/S0360-1285(99)00005-2)
- Winter F, Wartha C, Hofbauer H (1999) NO and N<sub>2</sub>O formation during the combustion of wood, straw, malt waste and peat. *Bioresour Technol* 70(1):39–49. [https://doi.org/10.1016/S0960-8524\(99\)00019-x](https://doi.org/10.1016/S0960-8524(99)00019-x)
- Wongsapai W, Achawangkul Y, Thepsaskul W, Daroon S, Fongsmootr T (2020) Biomass supply chain for power generation in southern part of Thailand. *Energy Rep* 6:221–227. <https://doi.org/10.1016/j.egy.2019.11.066>

Springer Nature or its licensor (e.g. a society or other partner) holds exclusive rights to this article under a publishing agreement with the author(s) or other rightsholder(s); author self-archiving of the accepted manuscript version of this article is solely governed by the terms of such publishing agreement and applicable law.